

Electronic Supplementary Information

Syntheses and structural investigation of some alkali metal ion-mediated $\text{LV}^{\text{V}}\text{O}_2^-$ (L^{2-} = Tridentate ONO ligands) species: DNA binding, photo-induced DNA cleavage and cytotoxic activities

Subhashree P. Dash,^a Alok K. Panda,^b Sagarika Pasayat,^a Rupam Dinda,^{*a} Ashis Biswas,^b Edward R. T. Tiekkink,^c Yogesh P. Patil,^d M. Nethaji,^d Werner Kaminsky,^e Subhadip Mukhopadhyay^f and Sujit K. Bhutia^f

^a*Department of Chemistry, National Institute of Technology, Rourkela 769008, Odisha, India.*

^b*School of Basic Science, Indian Institute of Technology Bhubaneswar, Bhubaneswar 751 013, Odisha, India.*

^c*Department of Chemistry, University of Malaya, 50603 Kuala Lumpur, Malaysia.*

^d*Department of Inorganic and Physical Chemistry, Indian Institute of Science, Bangalore 560012, India.*

^e*Department of Chemistry, University of Washington, Box 351700, Seattle, WA 98195, USA.*

^f*Department of Life Science, National Institute of Technology, Rourkela 769008, Odisha, India.*

Table of Contents

Table S1 Summary of intermolecular interactions ($A-H \dots B$; Å, °) operating in the crystal structures of **3**, **5-7**.

Table S2 Binding Constant (K_b) values for the interaction of CT-DNA with ligands.

Fig. S1 ^{51}V NMR spectra of **1** in DMSO-d₆.

Fig. S2 Overlay diagram of the two independent complex anions in **3**. Molecules have been superimposed so that the five-membered chelate rings involving the V1 (red image) and V2 (blue image) atoms are superimposed.

Fig. S3 (a) A view of the supramolecular layer in the *ab*-plane in **3** sustained by an extensive network of O-H...O hydrogen bonds shown as orange dashed lines. For clarity, only the chelate rings of the anions are illustrated, and (b) Unit cell contents for **3** viewed in projection down the *b*-axis. The O-H...O and C-H...O(hydroxy) hydrogen bonds are shown as orange and blue dashed lines, respectively.

Fig. S4 Overlay diagram of the two independent complex anions in **5**. Molecules have been superimposed so that the C1-C6 ring (red image) and C16-C21 ring (blue image) are superimposed.

Fig. S5 (a) Crystal packing in **5**: Layer in the *ab*-plane mediated by μ -O bridges. For clarity, only the chelate rings of the anions are illustrated, and (b) Unit cell contents for **5** viewed in projection down the *b*-axis. The O-H...O hydrogen bonds are shown as orange dashed lines.

Fig. S6 Crystal packing in **6**: View in projection down the *b*-axis showing the unit cell contents. The O-H...O, O-H...N, C-H...O and C-H... π interactions are shown as orange, blue, green and purple dashed lines, respectively.

Fig. S7 Crystal packing in **7**. (a) Layer in the *ab*-plane sustained by O-H...O and O-H...N hydrogen bonds shown as orange and blue dashed lines, respectively. For clarity, only the chelate rings of the anions are illustrated, and (b) Unit cell contents viewed in projection down the *b*-axis.

Fig. S8 Electronic absorption spectra of **1** (a), **2** (b), **3** (c), **4** (d), **5** (e) and **8** (f) (25 μ M each) upon the titration of CT-DNA (0 – 100 μ M) in 10 mM Tris-HCl buffer (pH 8.0) containing 10% DMF. Arrow shows the changes in absorbance with respect to an increase in the CT-DNA concentration. The inset shows the linear fit of $[DNA]/(\epsilon_a - \epsilon_f)$ vs [DNA] and binding constant (K_b) was calculated using Eq.1.

Fig. S9 Electronic absorption spectra of **H₂L¹** (a), **H₂L²** (b), **H₂L³** (c), **H₂L⁴** (d), **H₂L⁵** (e) and **H₂L⁶** (f) (25 μ M each) upon the titration of CT-DNA (0 – 350 μ M) in 10 mM Tris-HCl buffer (pH 8.0) containing 10% DMF. The inset shows the linear fit of $[DNA]/(\epsilon_a - \epsilon_f)$ vs [DNA] and binding constant (K_b) was calculated using Eq.1

Fig. S10 Derivative plot of thermal denaturation of CT-DNA (160 μ M) in absence and presence of **1-8** (100 μ M). The experiment was done in 10 mM Tris-HCl buffer (pH 8.0) containing 10% DMF. Inset shows the thermal denaturation derivate plot for **6** and **7** which showed ~ 2 °C shift in T_m as compared to CT-DNA.

Fig. S11 Circular dichroism spectra of CT-DNA (160 μ M) in the presence and absence of complexes in 10 mM Tris-HCl buffer (pH 8.0): **1** and **2** (a), **3** and **4** (b), **5** and **8** (c). The path length of the cuvette was 2 mm.

Fig. S12 (a) Gel diagram showing concentration dependent DNA cleavage by **1-8**; 300 ng of SC pUC19 DNA at different concentrations of the complexes [1–500 μ M in 10 mM Tris-HCl buffer (pH 8.0) containing 1% DMF] was photo-irradiated with UVA at 350 nm for 3 h. Lanes **1-9**: 1, 2.5, 5.0, 7.5, 10, 50, 75, 100 and 500 μ M of **1-8**. (b) Concentration dependent DNA cleavage by **1-8**; 300 ng of SC pUC19 DNA at different concentration of the complexes [1–500 μ M in 10 mM Tris HCl buffer (pH 8.0) containing 1% DMF] was photo-irradiated with UVA at 350 nm for 3 h. The net DNA cleavage percent was calculated using Eq.2. Inset shows a bar diagram representation of the net DNA cleavage of different complexes at 10 and 100 μ M.

Fig. S13 (a) Gel diagram showing concentration dependent DNA cleavage by **1-8**; 300 ng of SC pUC19 DNA at different concentrations of the complexes [1–500 μ M in 10 mM phosphate buffer (pH 7.8) containing 1% DMF] was photo-irradiated with UVA at 350 nm for 3 h. Lanes **1-9**: 1, 2.5, 5.0, 7.5, 10, 50, 75, 100 and 500 μ M of **1-8**. (b) Concentration dependent DNA cleavage by **1-8**; 300 ng of SC pUC19 DNA at different concentration of the complexes [1–500 μ M in 10 mM

phosphate buffer (pH 7.8) containing 1% DMF] was photo-irradiated with UVA at 350 nm for 3 h. The net DNA cleavage percent was calculated using Eq.2. Inset shows a bar diagram representation of the net DNA cleavage of different complexes at 10 and 100 μ M

Fig. S14 Effect of DMF (10%) and ligands on the photo-induced cleavage of SC pUC19 DNA. 300 ng SC pUC19 DNA was photo-irradiated in presence of 10% DMF and various ligands (100 μ M) with UVA at 350 nm for 3 h. Lane 1, DNA in presence of 10% DMF; Lane 2, DNA + H₂L¹; Lane 3, DNA + H₂L²; Lane 4, DNA + H₂L³; Lane 5, DNA + H₂L⁴; Lane 6, DNA + H₂L⁵; Lane 7, DNA + H₂L⁶.

Fig. S15 Gel diagram depicting cleavage of SC pUC19 DNA by **1–8** in presence of various additives in 50 mM Tris-HCl buffer (pH 8.0) containing 10% DMF. SC pUC19 DNA (300 ng) in the presence of various additives was photo-irradiated at 350 nm for 3 h with **1–8** (100 μ M). The additive concentrations were: sodium azide (0.5 mM), L-histidine (0.5 mM), KI (0.5 mM) and D-mannitol (0.5 mM). Lane 1, DNA + complex; Lane 2, DNA + complex + sodium azide; Lane 3, DNA + complex + L-histidine; Lane 4, DNA + complex + KI; Lane 5, DNA + complex + D-mannitol

Fig. S16 Cleavage of SC pUC19 DNA by **1–4** (a) and **5–8** (b) in presence of various additives in 50mM Tris-HCl buffer (pH 8.0) containing 10% DMF. SC pUC19 DNA (300 ng) in the presence of various additives was photo-irradiated at 350 nm for 3 h with **1–8** (100 μ M). The additive concentrations were: sodium azide (0.5 mM), L-histidine (0.5 mM), KI (0.5 mM) and D-mannitol (0.5 mM).

Fig. S17 The plot represents the linear fit of log [(F₀-F)/F] vs log [Q] for **6** (a) and **7** (b) and the binding constant (K_{BSA}) was estimated using Eq.4. Here, [Q] stands for [quencher (complexes)].

Fig. S18 SDS-PAGE profile of cleavage of BSA in presence of complexes **1–8** (100 μ M) in (a) UVA light of 350 nm (84 W) and (b) dark. Lane 1, Molecular marker; Lane 2, BSA only; Lane 3, BSA + **1** (100 μ M); Lane 4, BSA + **2** (100 μ M); Lane 5, BSA + **3** (100 μ M); Lane 6, BSA + **4** (100 μ M); Lane 7, BSA + **5** (100 μ M); Lane 8, BSA + **6** (100 μ M); Lane 9, BSA + **7** (100 μ M); Lane 10, BSA + **8** (100 μ M).

Fig. S19 Effect of ligand (H₂L⁵) on cell viability and growth: HeLa cells were treated with different concentrations of the test compound for 72 h and then cell viability was measured by MTT assay. Data reported as the mean \pm S.D. for n = 6 and compared against 10% (v/v) DMF treated control by using a Student's t-test. (*significant compared control).

Fig. S20 Study of apoptosis by morphological changes in nuclei of HeLa cells: HeLa cells, from control and treated groups, were fixed with 3.7% formaldehyde for 15 min, permeabilized with 0.1% Triton X-100 and stained with 1 μ g/ml DAPI for 5 min at 37 °C. The cells were then washed with PBS and examined by fluorescence microscopy (Olympus IX 71) (200 \times). HeLa cells were treated with 225 μ M of ligand (H₂L⁵). Arrows showing the morphological changes in nuclei of HeLa cells were observed on applying ligand (H₂L⁵) in comparison to the control group treated with 10% (v/v) DMF.

Fig. S21 ¹H NMR spectra of **1** (a), **5** (b), **6** (c) and **7** (d) in DMSO-d₆

Fig. S22 Electronic absorption spectra of **7** (2.5×10^{-5} M) in DMF.

Fig. S23 FTIR spectra of complex **6**.

Table S1: Summary of intermolecular interactions (A–H...B; Å, °) operating in the crystal structures of **3**, **5–7**.^a

A	H	B	A–H	H...B	A...B	A–H...B	Symmetry operation
3							
O1	H1O	N1	0.84	1.83	2.567(2)	146	<i>x, y, z</i>
O6	H6O	N3	0.84	1.83	2.571(2)	146	<i>x, y, z</i>
O1W	H1W1	O9	0.80	1.93	2.7126(19)	167	<i>x, y, z</i>
O1W	H1W2	O5	0.80	2.01	2.7486(19)	153	<i>x, y, -1+z</i>
O2W	H2W1	O3	0.80	2.09	2.886(2)	173	-1+x, <i>y, -1+z</i>
O2W	H2W2	O8W	0.80	2.04	2.817(2)	165	-1+x, <i>y, z</i>
O3W	H3W1	O7	0.80	2.24	2.972(2)	152	1- <i>x, 1-y, -z</i>
O3W	H3W1	O10	0.80	2.46	3.108(2)	139	1- <i>x, 1-y, -z</i>
O3W	H3W2	O9W	0.80	1.99	2.774(2)	165	<i>x, y, z</i>
O4W	H4W1	O8	0.80	2.06	2.831(2)	163	-1+x, <i>y, z</i>
O4W	H4W2	O7	0.80	2.31	3.088(2)	165	<i>x, y, z</i>
O5W	H5W1	O8W	0.80	1.97	2.736(2)	159	-1+x, <i>y, z</i>
O5W	H5W2	O2	0.80	2.14	2.937(2)	171	1- <i>x, -y, 1-z</i>
O6W	H6W1	O2	0.80	2.06	2.8552(19)	169	<i>x, y, -1+z</i>
O6W	H6W2	O3	0.80	2.39	3.079(2)	145	-1+x, <i>y, -1+z</i>
O6W	H6W2	O4	0.80	2.36	3.0187(19)	140	-1+x, <i>y, -1+z</i>
O7W	H7W1	O4	0.80	1.95	2.744(2)	173	<i>x, y, -1+z</i>
O7W	H7W2	O6W	0.80	2.04	2.825(2)	166	1- <i>x, -y, -z</i>
O8W	H8W1	O8	0.80	2.41	3.073(2)	141	<i>x, y, z</i>
O8W	H8W1	O9	0.80	2.27	2.959(2)	145	<i>x, y, z</i>
O8W	H8W2	O7W	0.80	1.97	2.760(2)	169	<i>x, y, z</i>
O9W	H9W1	O10	0.80	1.97	2.767(2)	178	<i>x, y, z</i>
O9W	H9W2	O2W	0.80	1.99	2.785(2)	171	1+x, <i>y, z</i>

C8	H8	O6	0.95	2.35	3.274(2)	165	$1+x, y, z$
C22	H22	O1	0.95	2.30	3.240(2)	168	x, y, z

5

O1W	H1W1	O2	0.84(2)	2.43(3)	3.038(3)	130(2)	x, y, z
O1W	H1W1	O4	0.84(2)	2.48(2)	3.274(3)	159(2)	x, y, z
O1W	H1W2	O4	0.84(3)	1.89(2)	2.723(3)	170(3)	$1-x, 1-y, 1-z$
O2W	H2W1	O6	0.85(3)	1.96(3)	2.776(3)	160(3)	$-x, -1-y, 1-z$
O2W	H2W2	O7	0.85(3)	2.15(3)	2.986(3)	171(2)	$x, -1+y, z$

6

O1W	H1W1	O1	0.85(3)	2.11(4)	2.931(3)	162(3)	$\frac{1}{2}-x, \frac{1}{2}+y, z$
O1W	H1W2	N1	0.837(18)	2.01(2)	2.815(3)	162(4)	$1-x, -y, -z$
C5	H5	O4	0.93	2.54	3.439(3)	164	$1-x, -y, -z$
C7'	H72	Cg1	0.96	2.56	3.477(3)	159	$1\frac{1}{2}-x, -\frac{1}{2}+y, z$
O2W	H2W2	O3	0.863(14)	2.44(5)	2.852(4)	110(4)	$\frac{1}{2}-x, \frac{1}{2}+y, z$

The O2W-water molecule atom lies in a pocket comprising the O3 atom, see above, and the O1W (separation 3.313(2) Å), O3 (3.261(2) Å) and O4 (3.364(2) Å) atoms.

Cg1 is the centroid of the (C8-C13) ring

7

O1W	H1W1	O1	0.82(3)	2.17(3)	2.975(2)	165(2)	x, y, z
O1W	H1W2	O4W	0.83(3)	1.97(3)	2.787(2)	166(3)	$1-x, -y, 2-z$
O2W	H2W1	O3	0.84(3)	2.08(3)	2.885(2)	162(3)	$-1+x, y, z$
O2W	H2W2	O4W	0.83(3)	1.98(3)	2.809(2)	173(3)	x, y, z
O3W	H3W1	O2W	0.83(3)	2.24(3)	3.015(3)	156(3)	$-x, -y, 2-z$
O3W	H3W2	N2	0.83(3)	2.26(3)	2.991(3)	147(3)	$1-x, 1-y, 2-z$
O4W	H4W1	N1	0.834(13)	1.982(13)	2.808(2)	171(2)	$-1+x, -1+y, -1+z$
O4W	H4W2	O2	0.84(2)	2.06(2)	2.876(2)	166(2)	x, y, z

Table S2 Binding Constant (K_b) values for the interaction of CT-DNA with ligands

Complex	Binding Constant (K_b) ^a (M^{-1})
$\mathbf{H_2L}^1$	1.29×10^3
$\mathbf{H_2L}^2$	7.74×10^3
$\mathbf{H_2L}^3$	8.79×10^3
$\mathbf{H_2L}^4$	3.82×10^3
$\mathbf{H_2L}^5$	1.09×10^3
$\mathbf{H_2L}^6$	4.57×10^3

^aDNA binding constant by UV-vis spectral method.

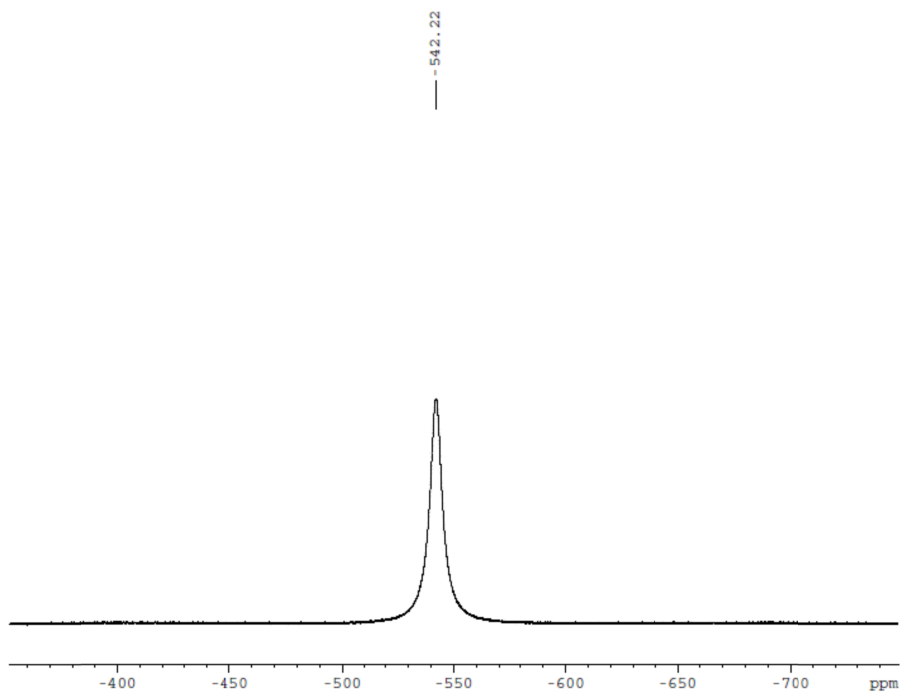


Fig. S1

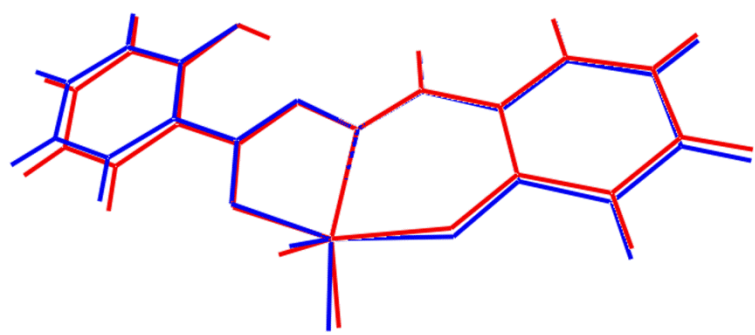
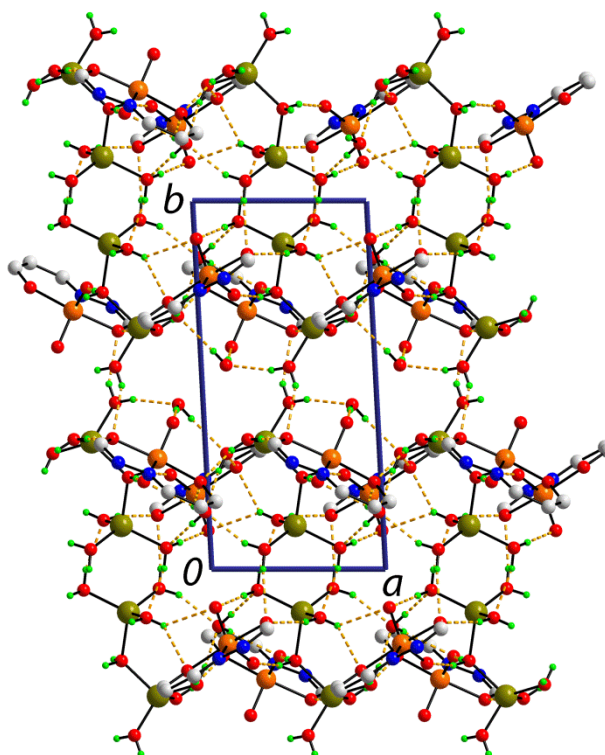
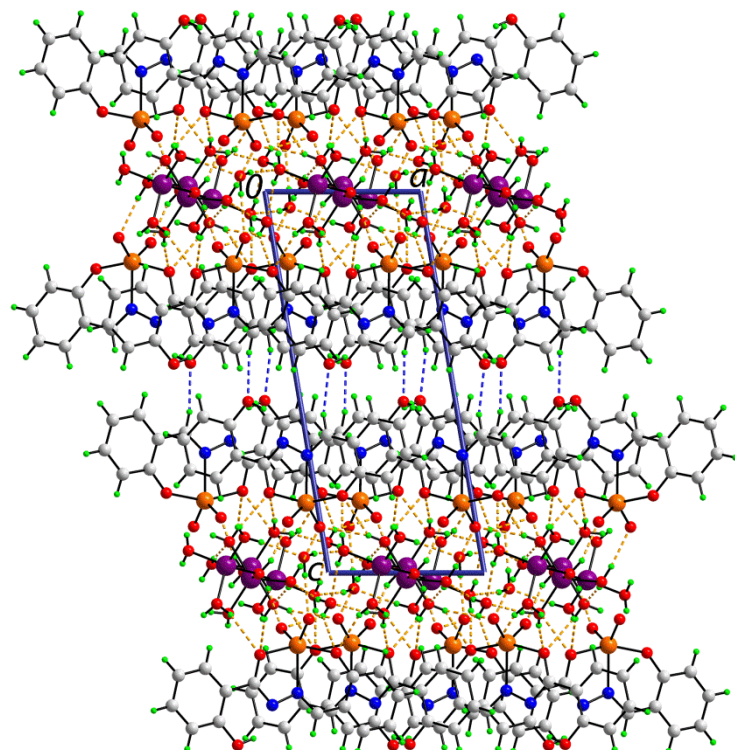


Fig. S2



(a)



(b)

Fig. S3

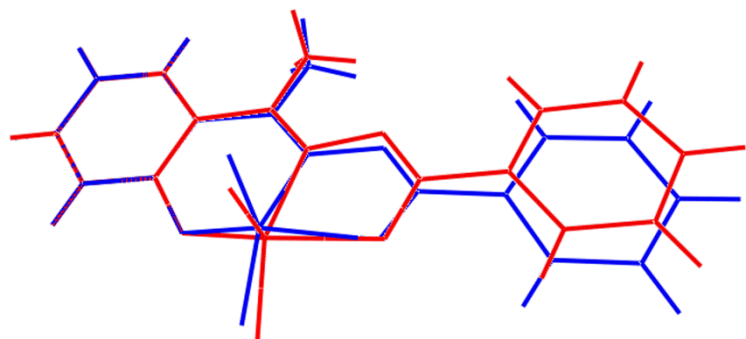
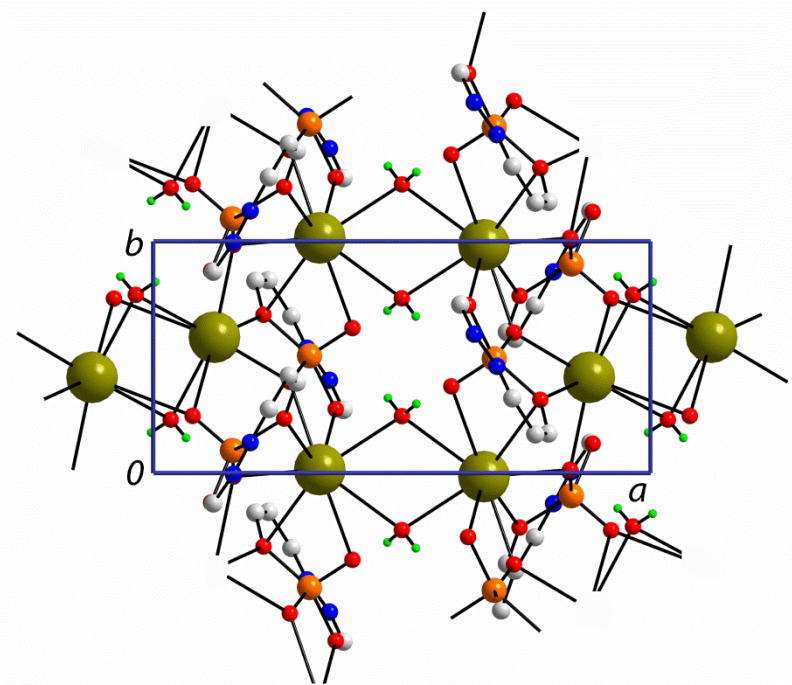
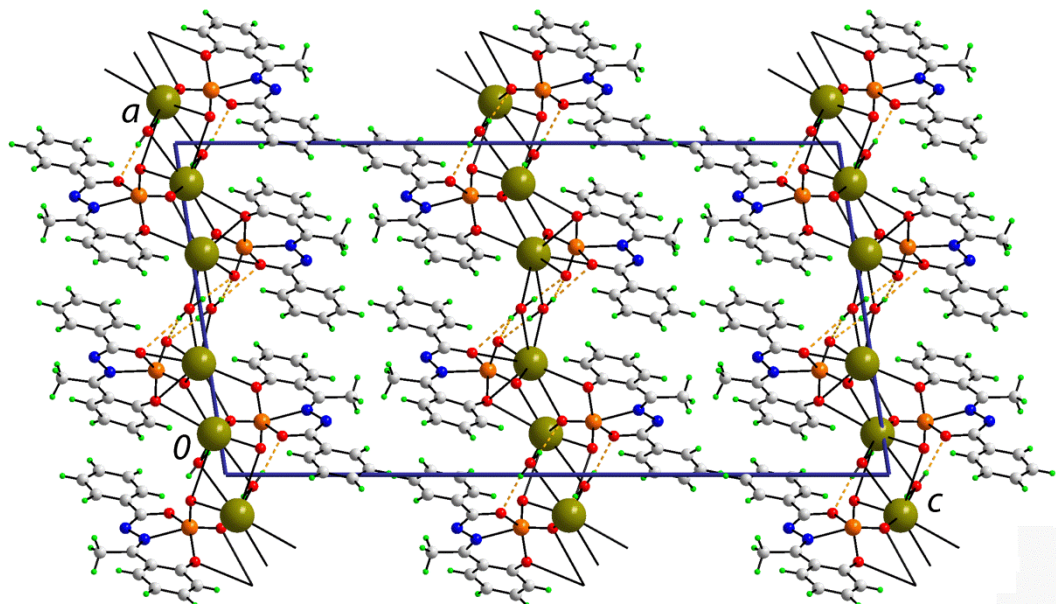


Fig. S4



(a)



(b)

Fig. S5

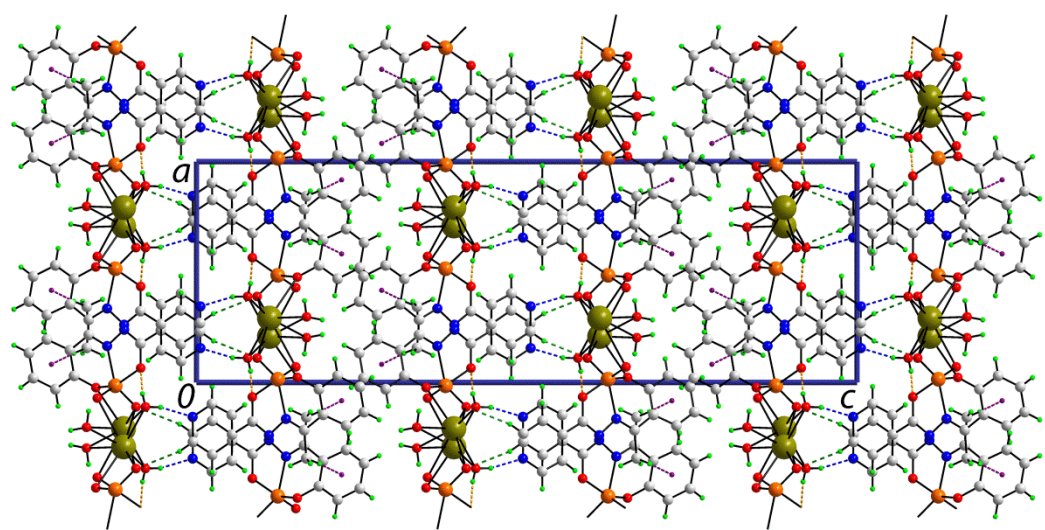
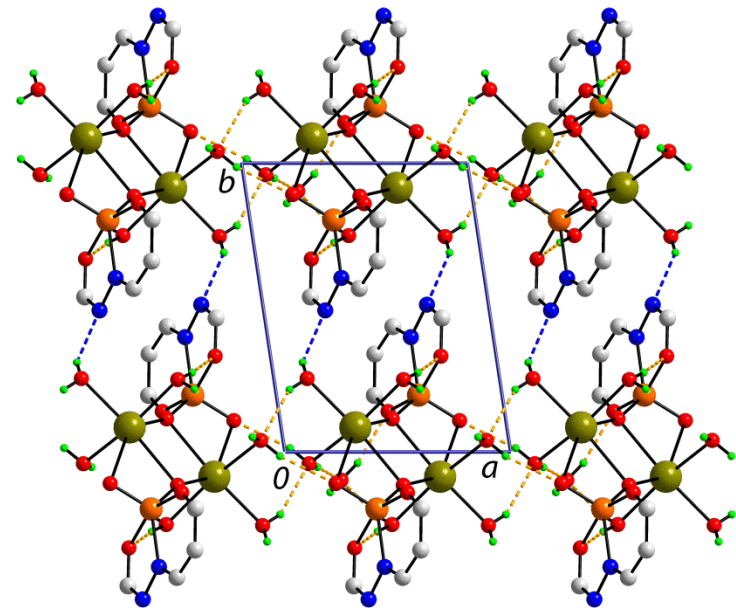
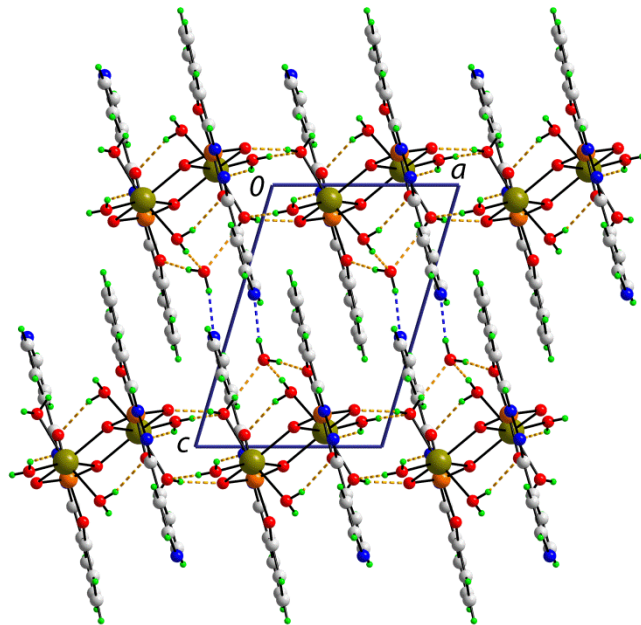


Fig. S6

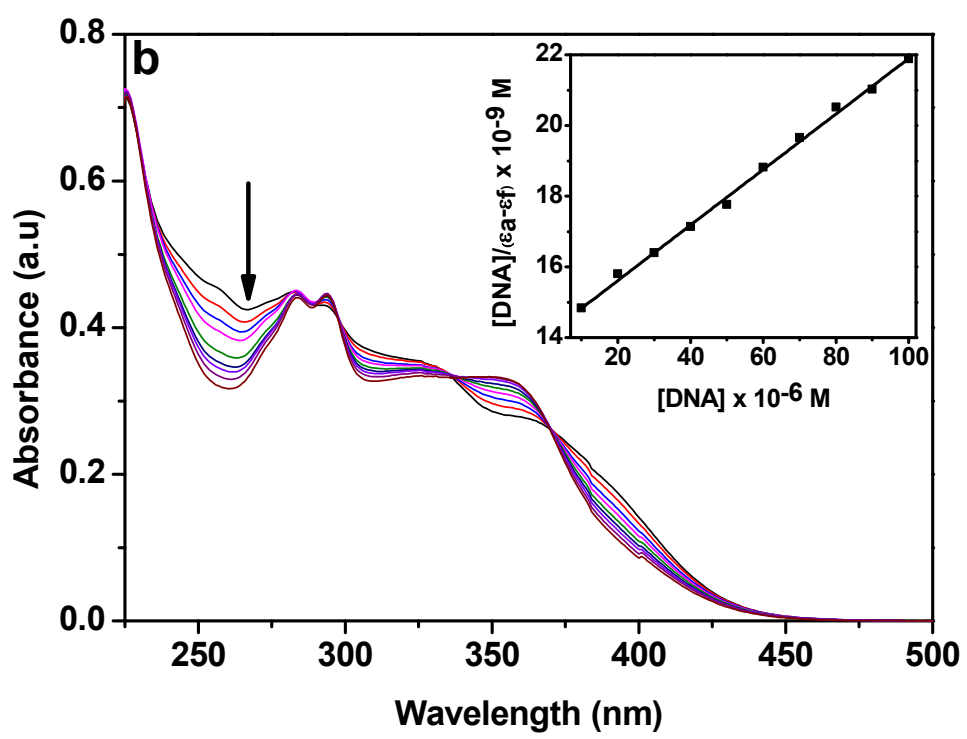
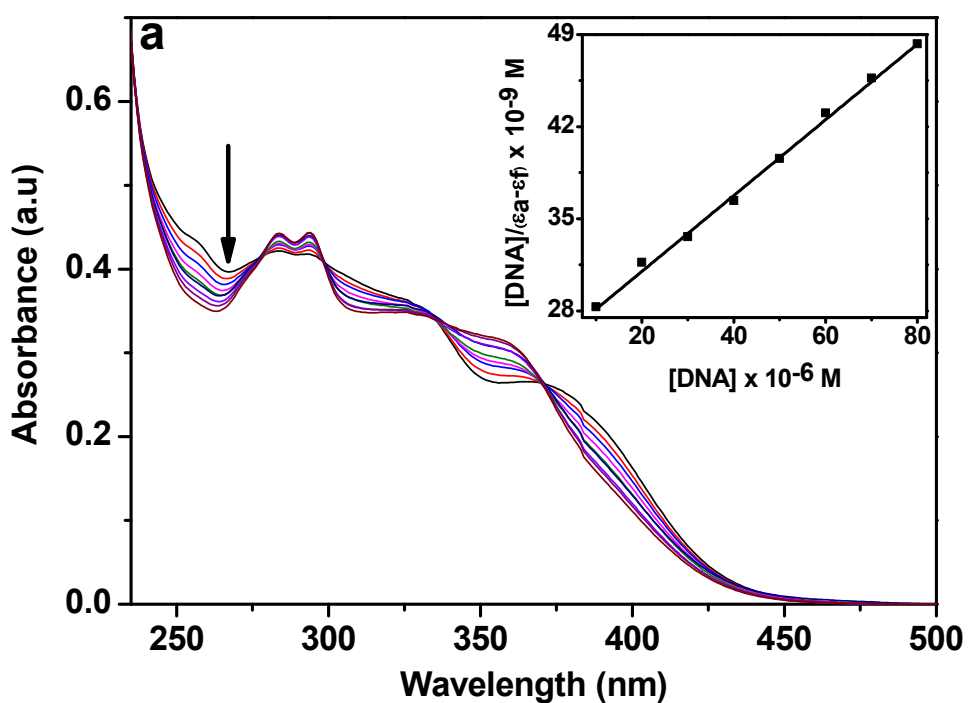


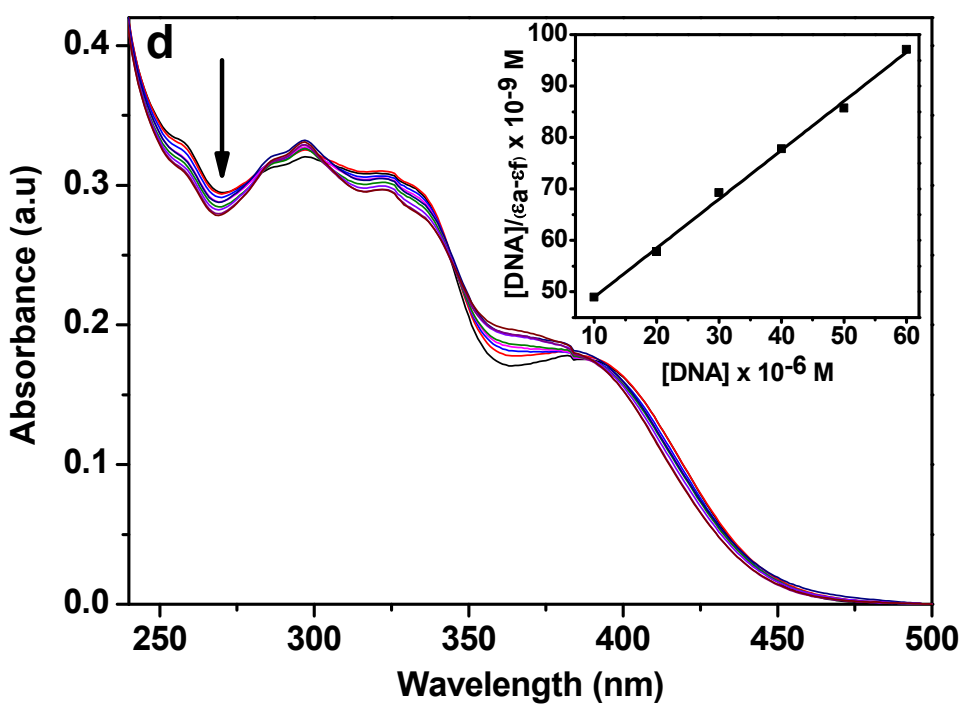
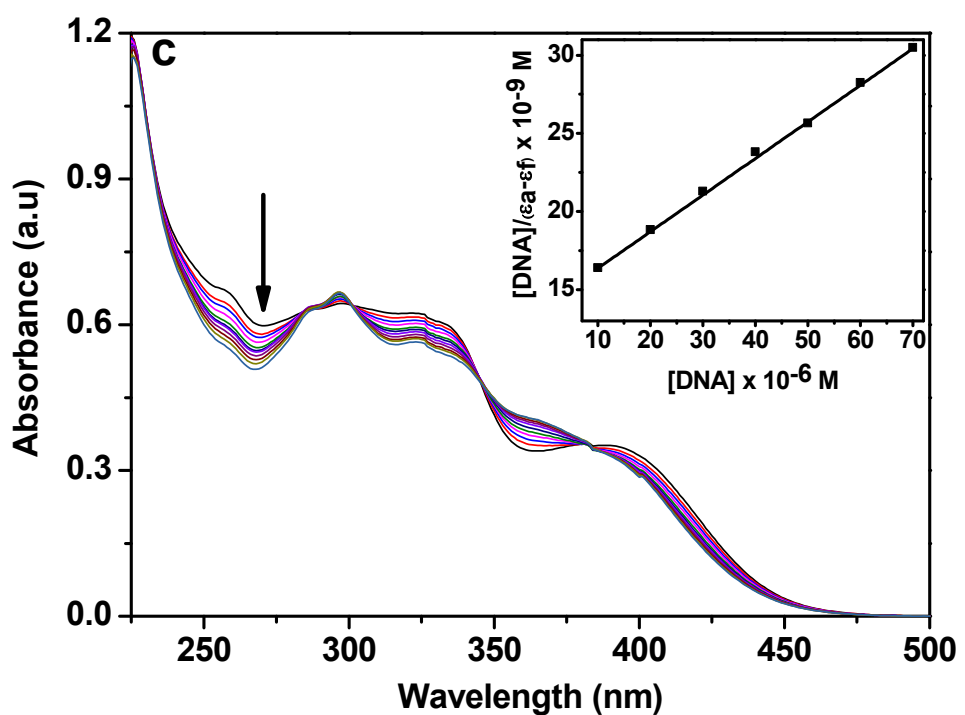
(a)



(b)

Fig. S7





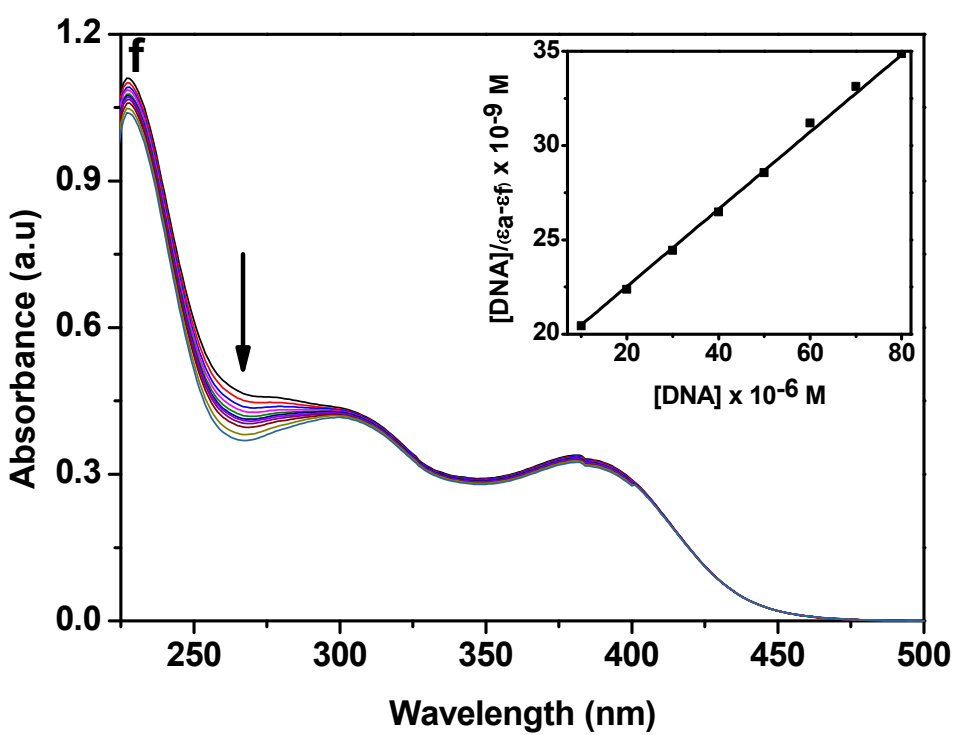
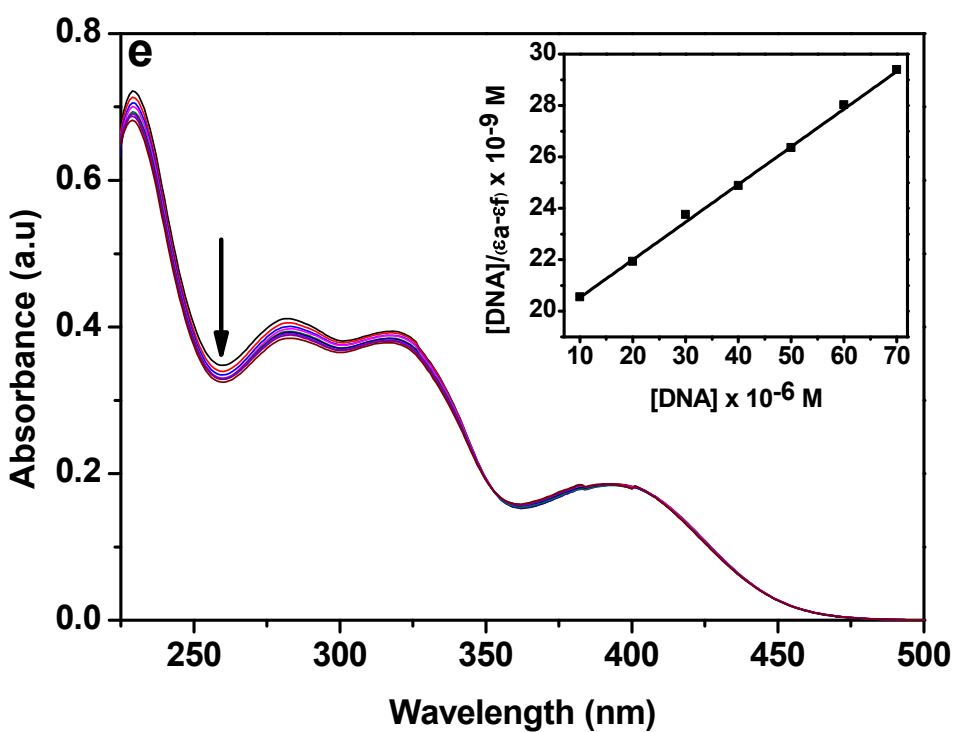
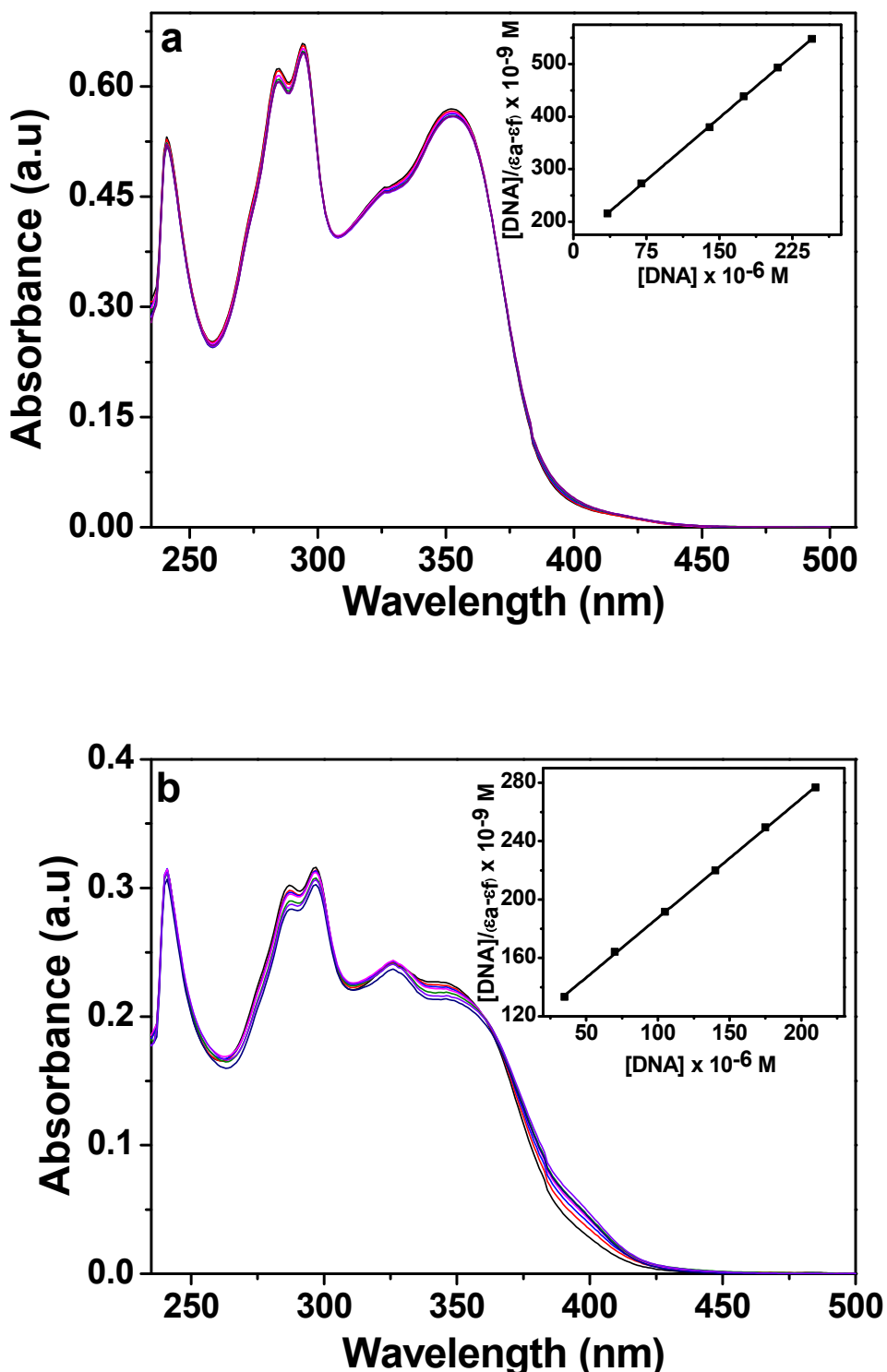
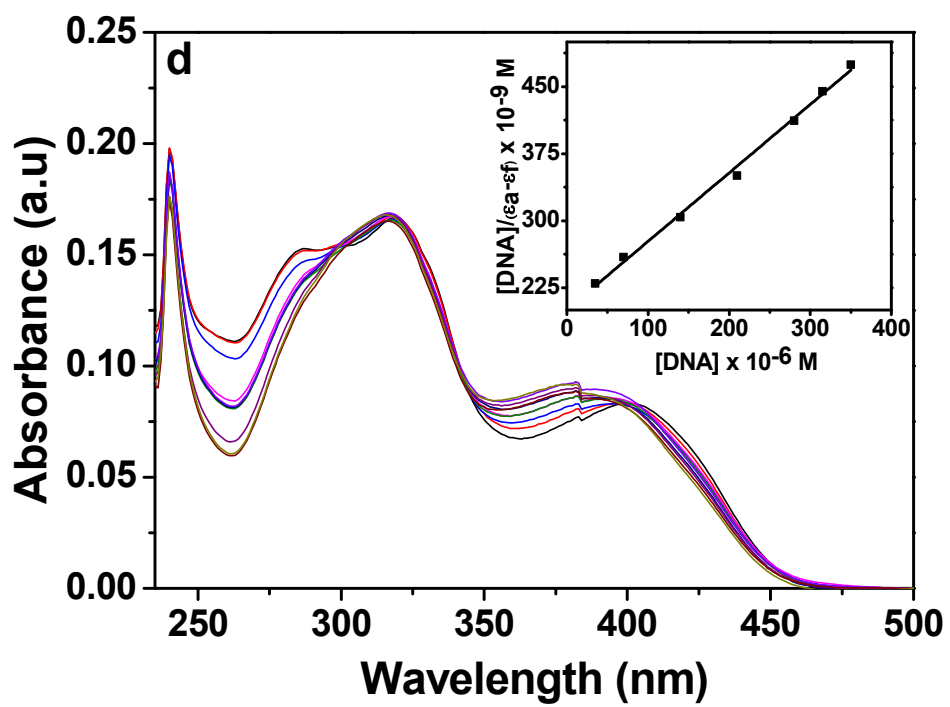
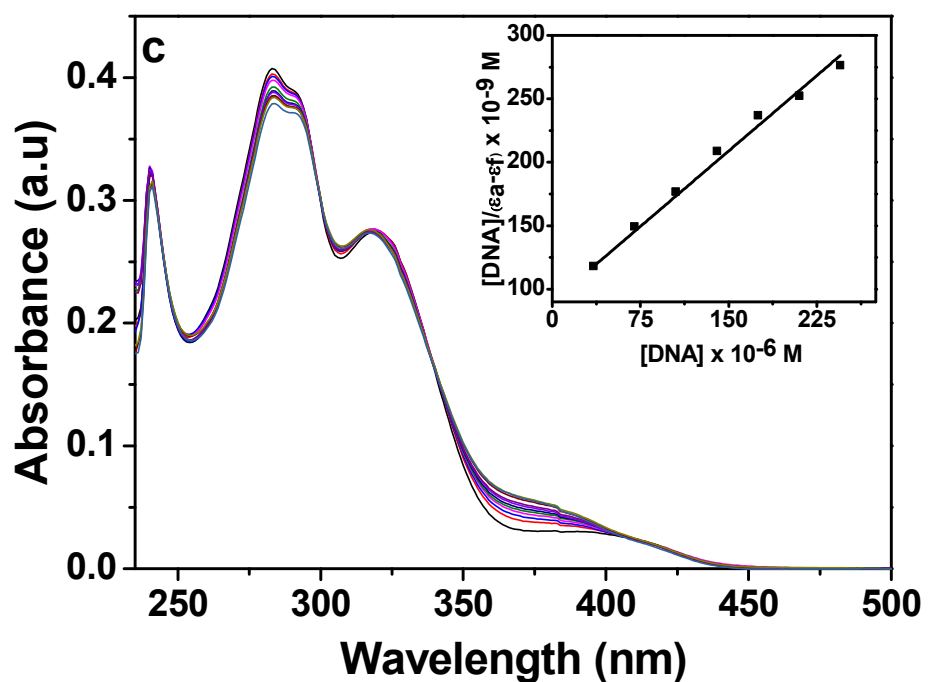


Fig. S8





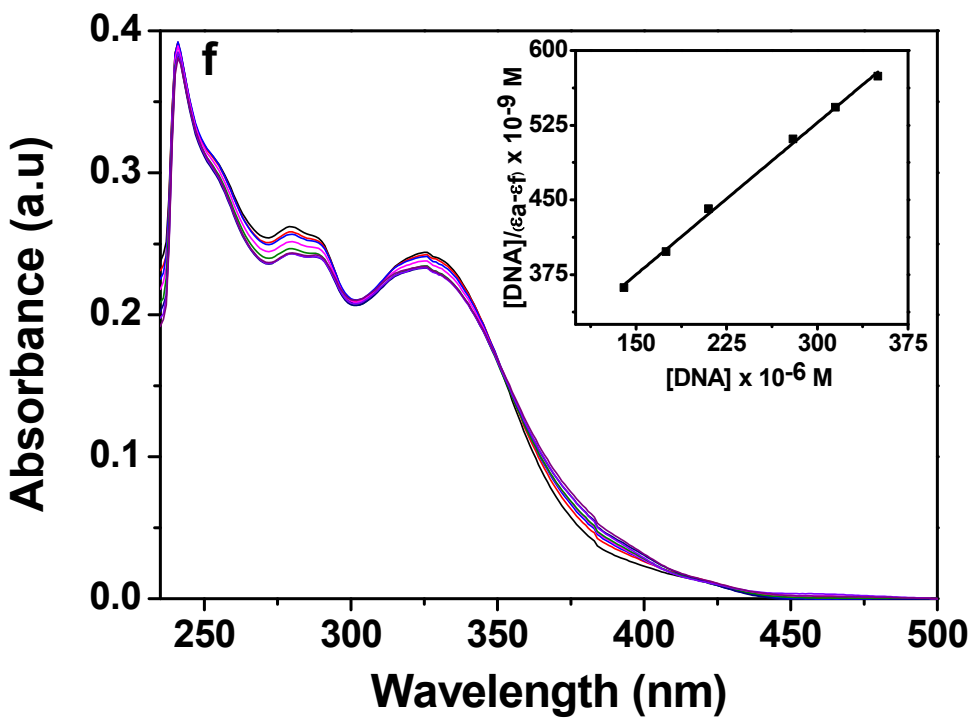
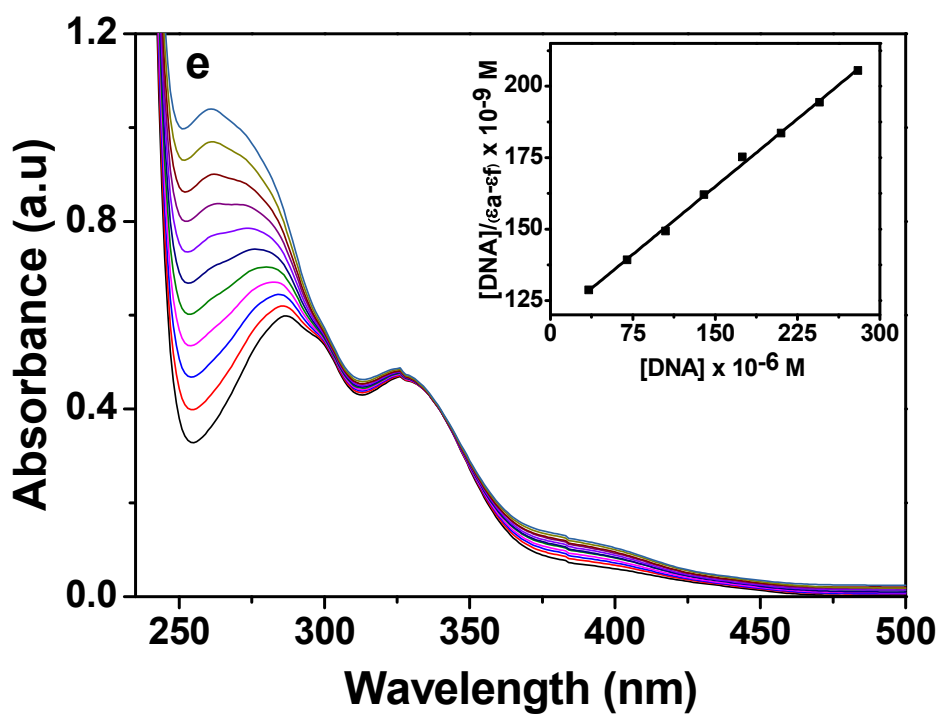


Fig. S9

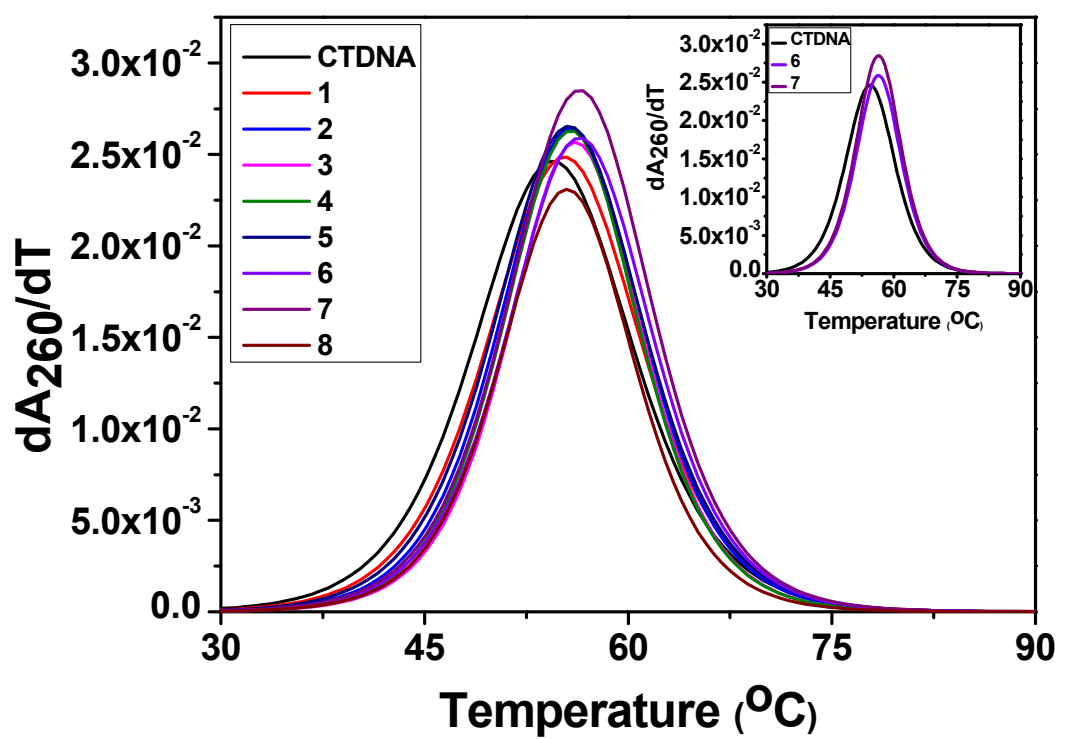
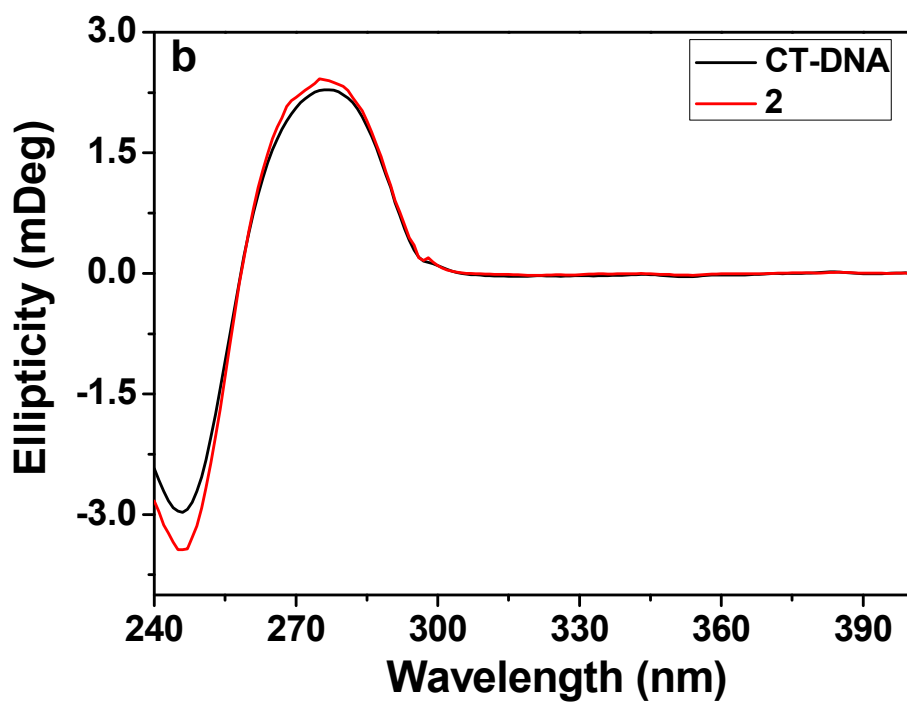
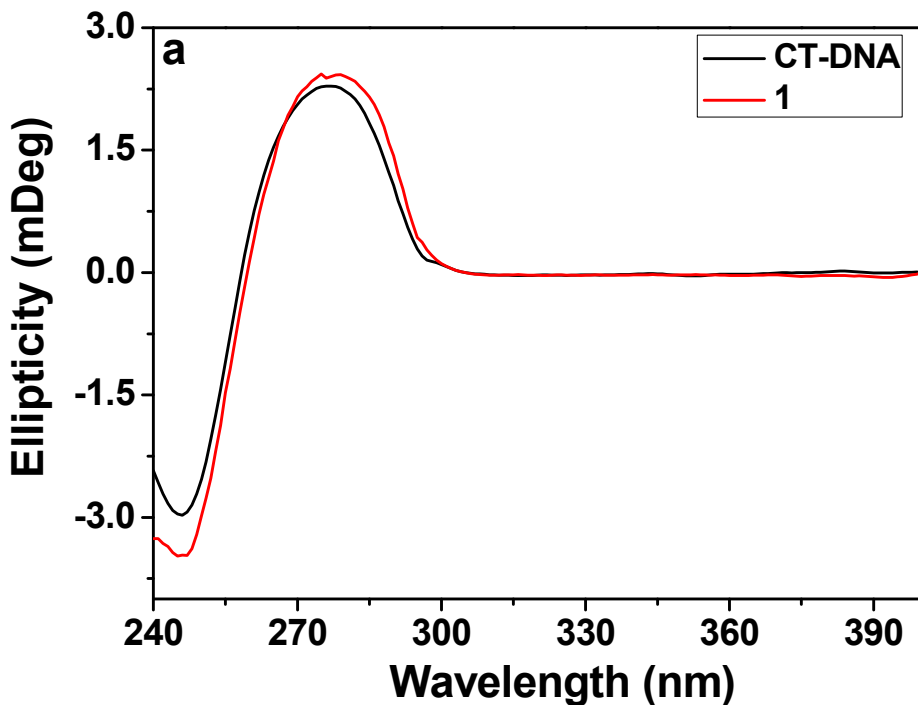
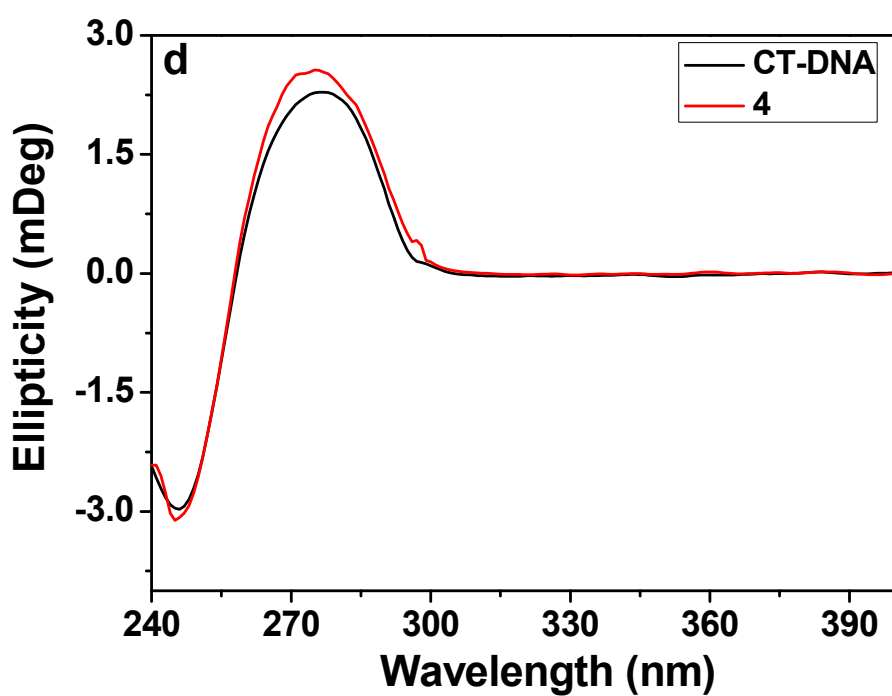
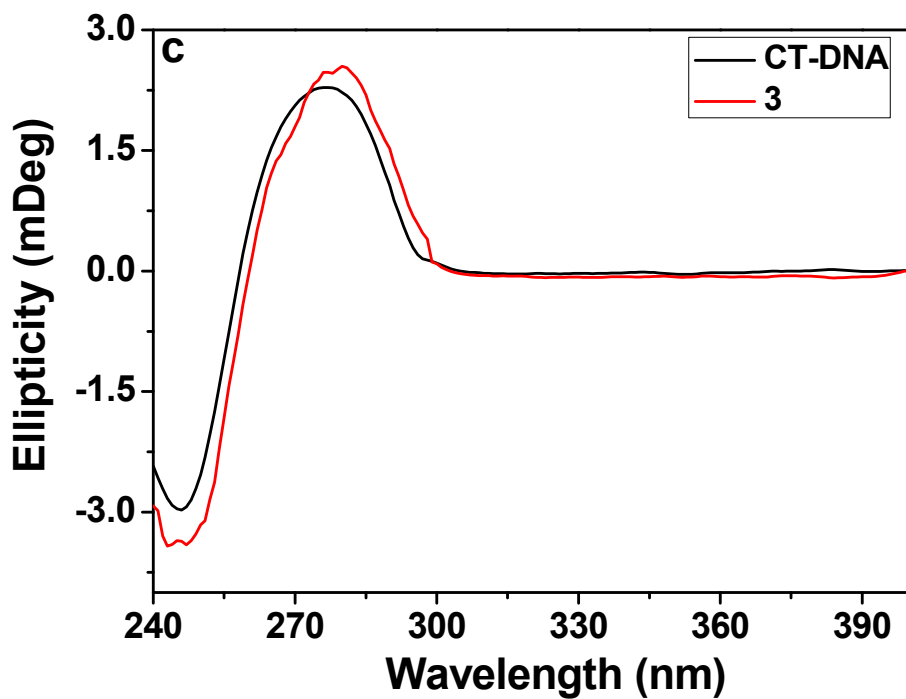


Fig. S10





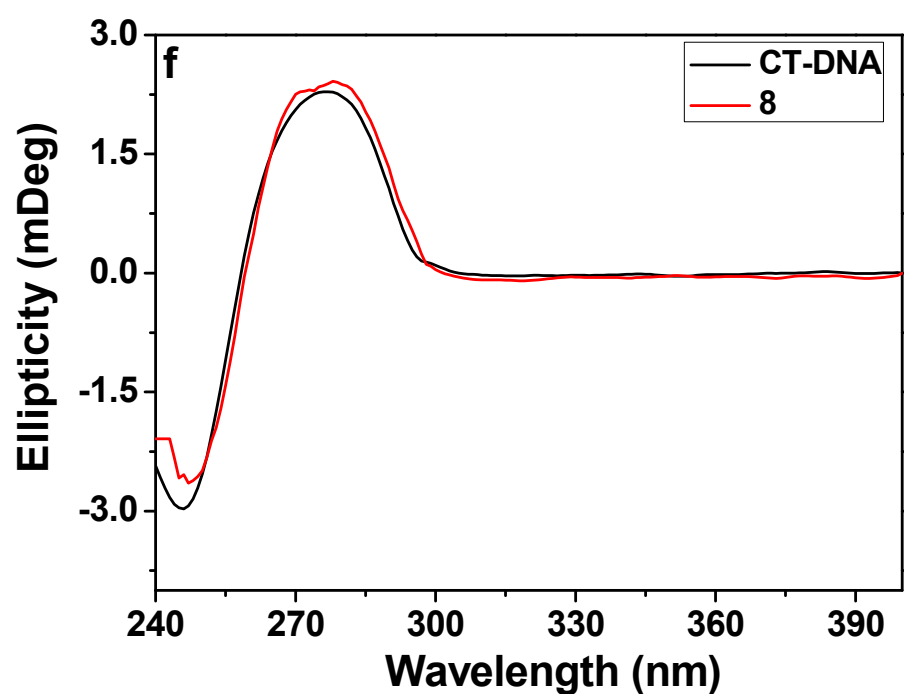
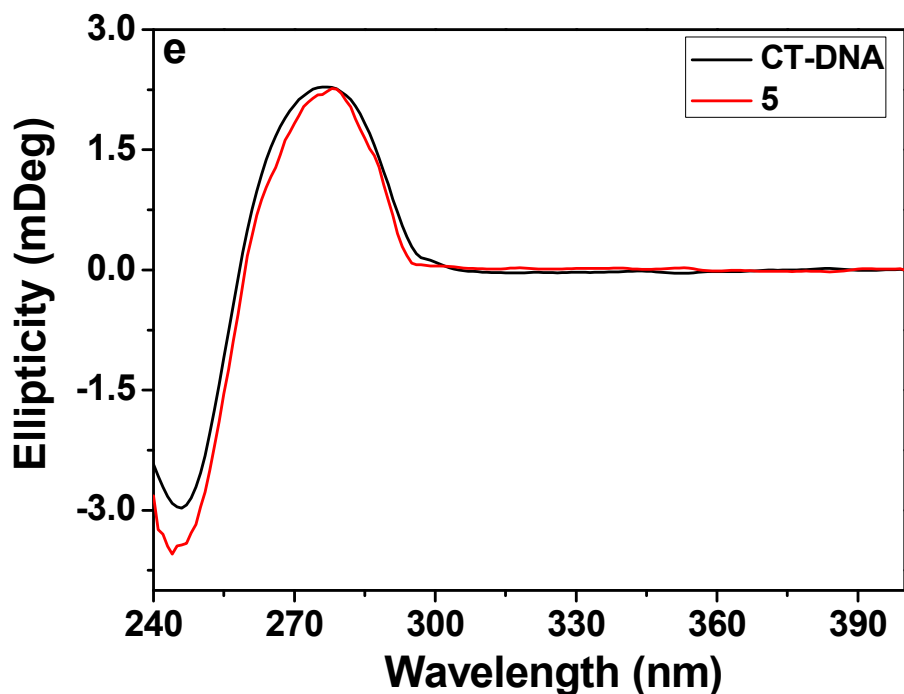


Fig. S11

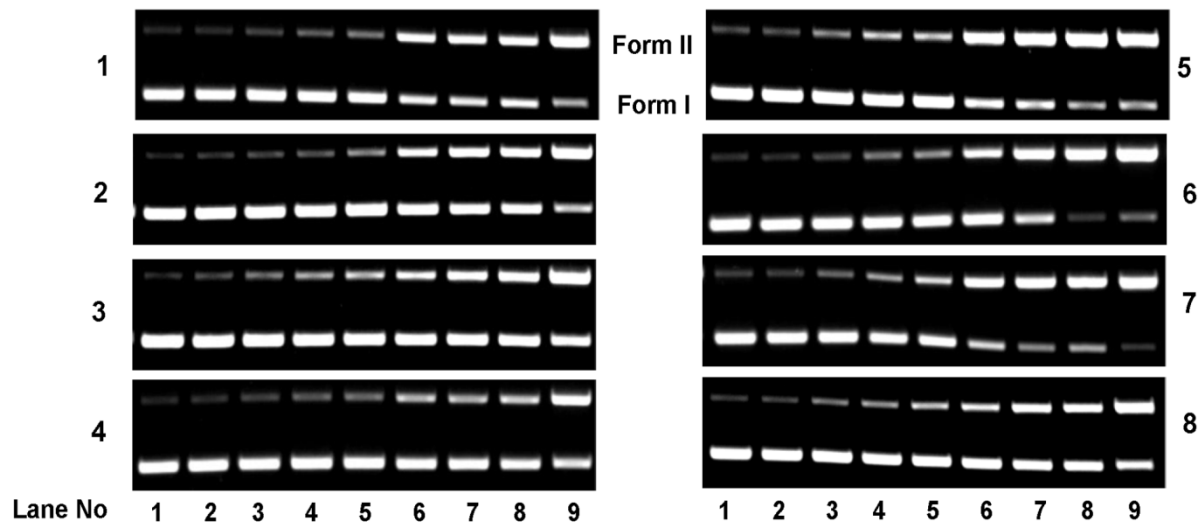
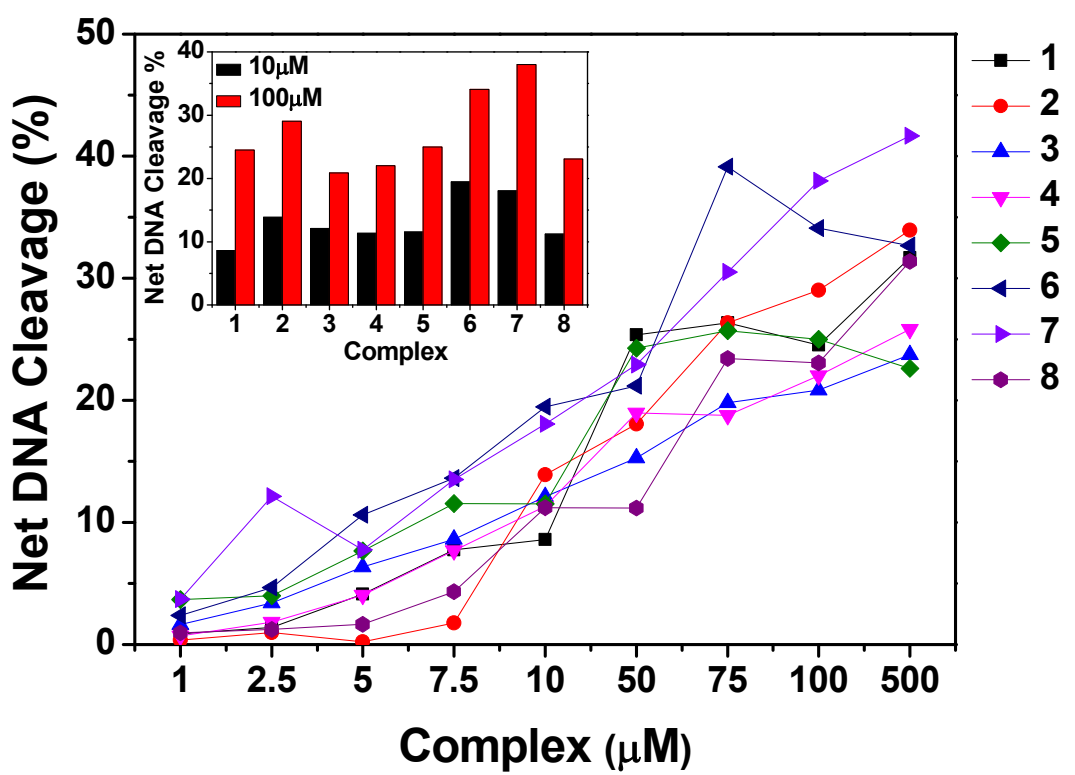
a**b**

Fig. S12

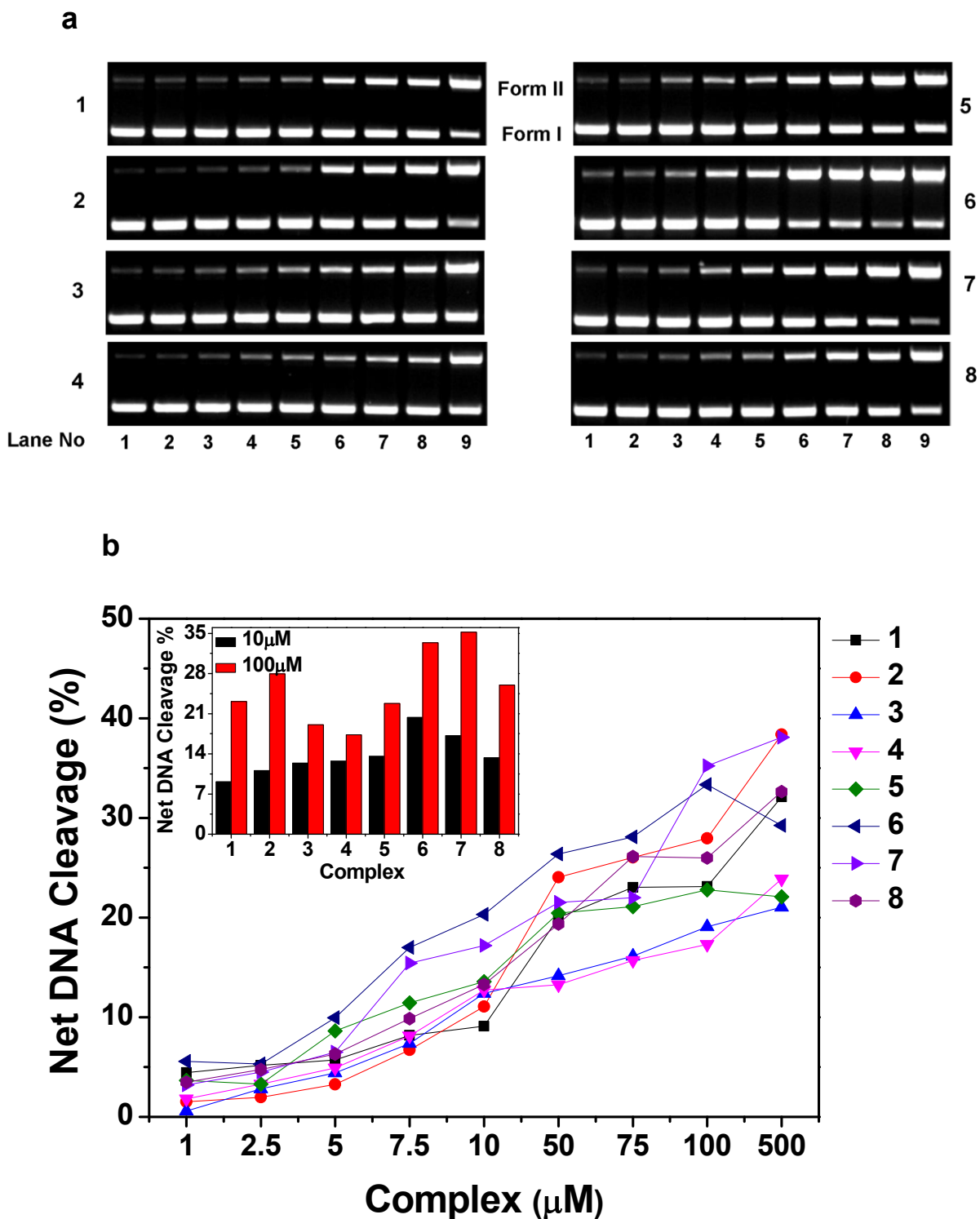


Fig. S13



Fig. S14

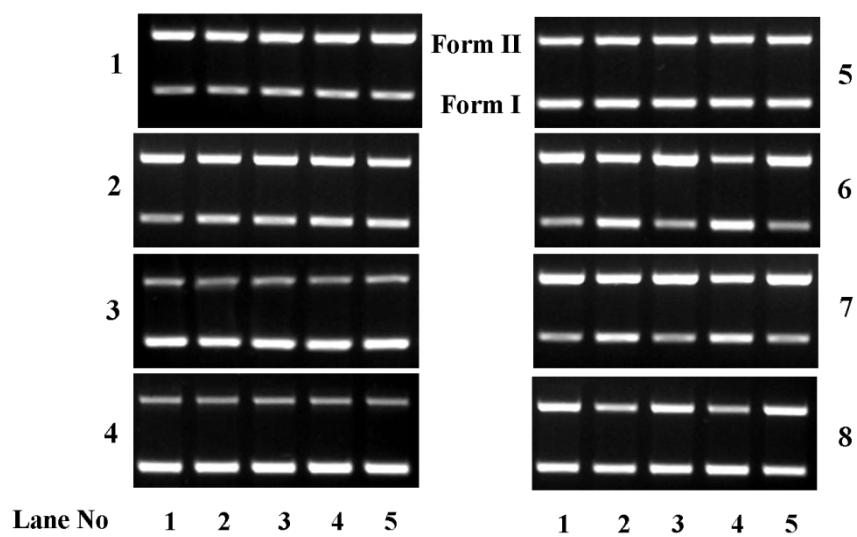


Fig. S15

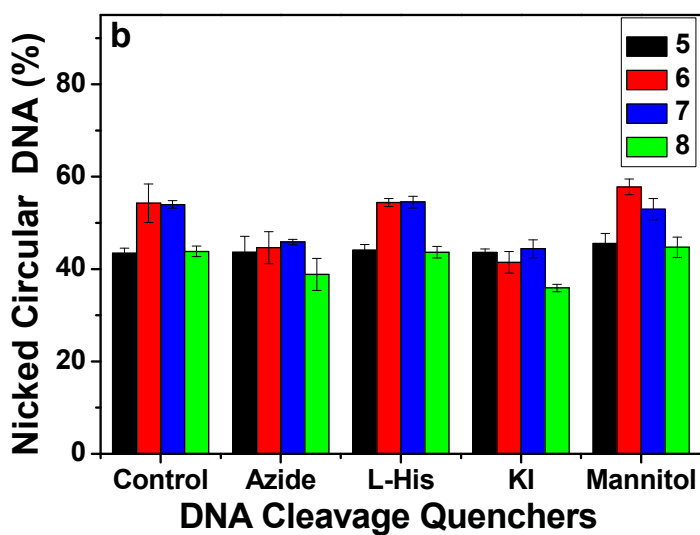
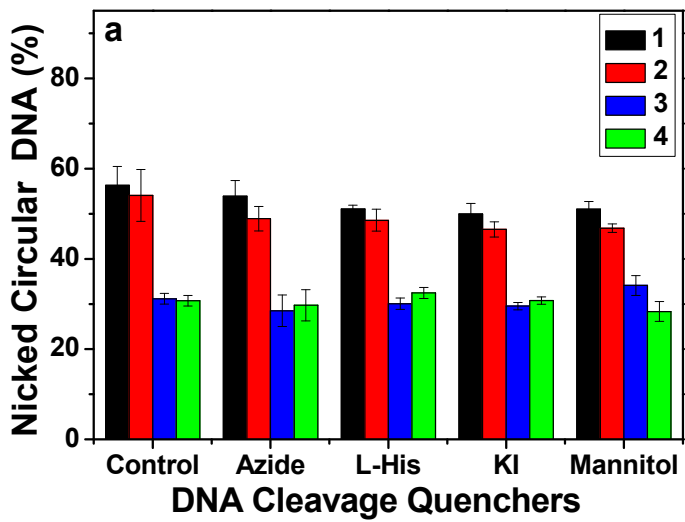


Fig. S16

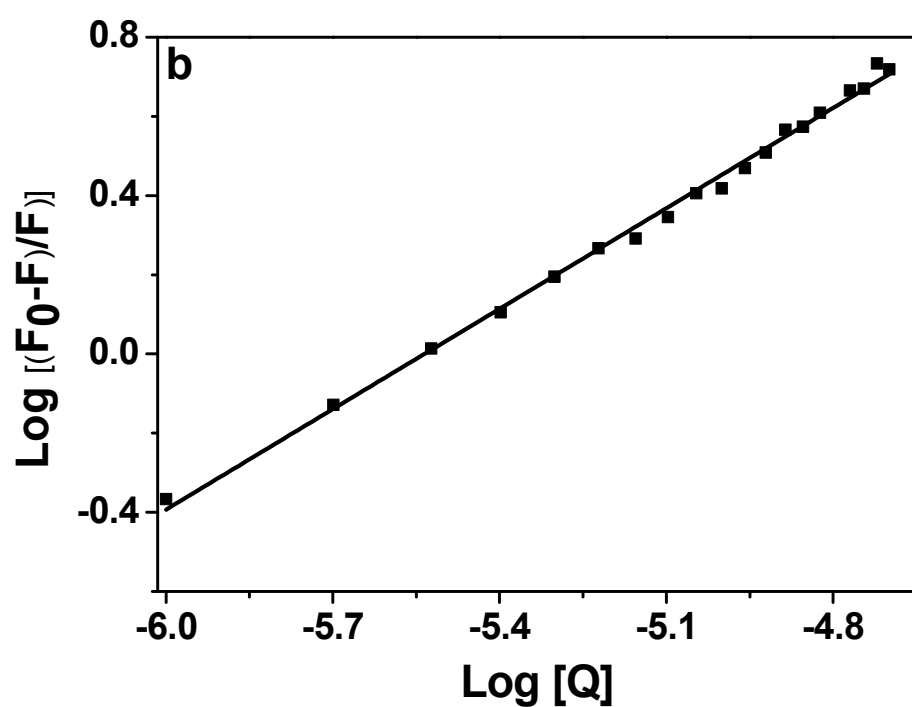
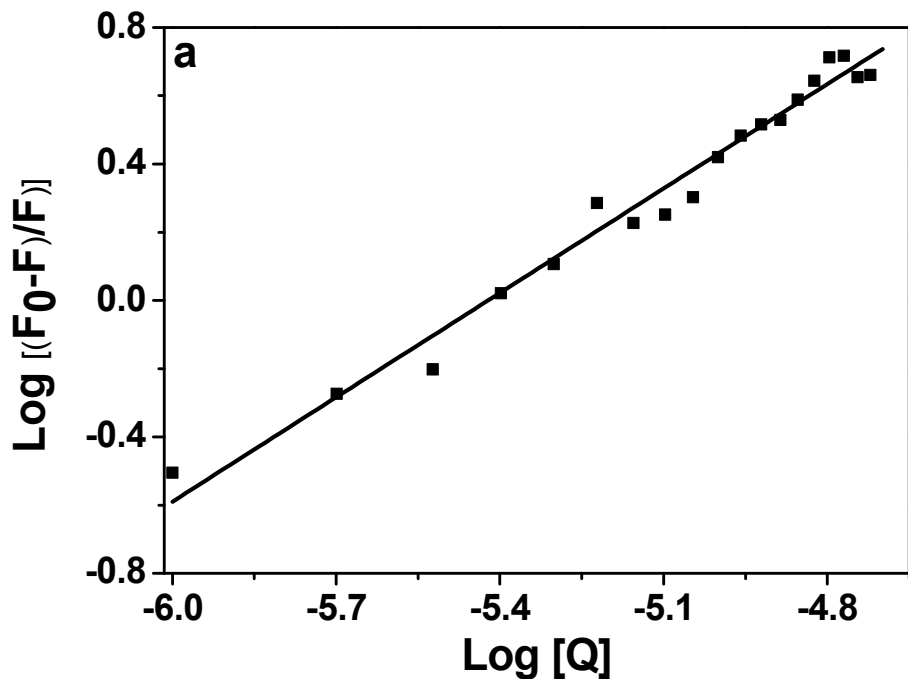


Fig. S17

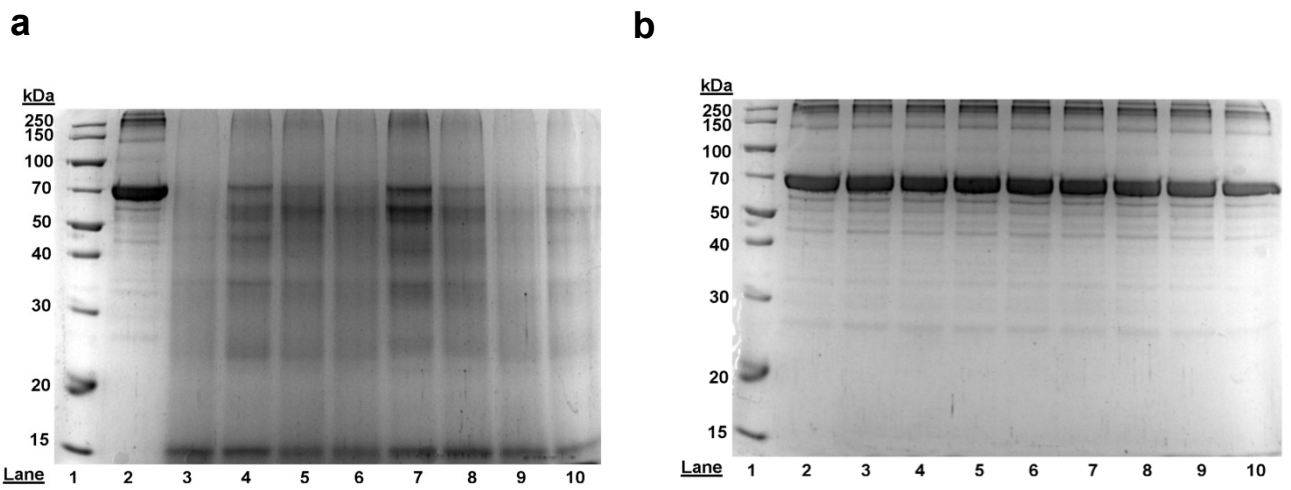


Fig. S18

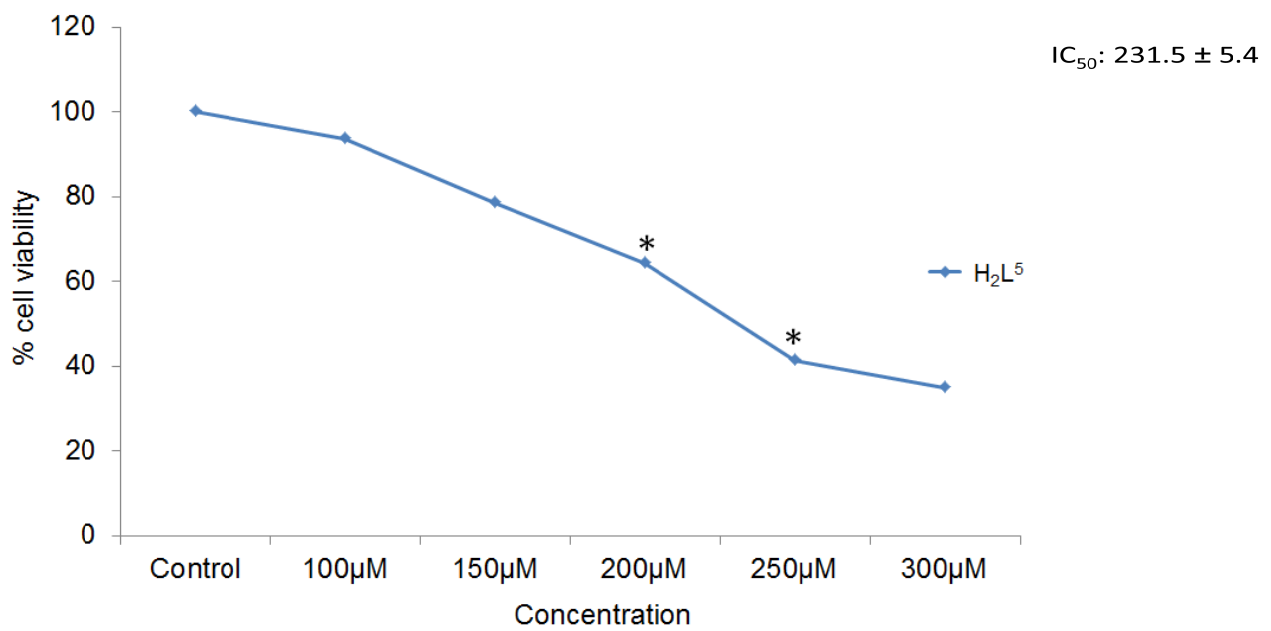
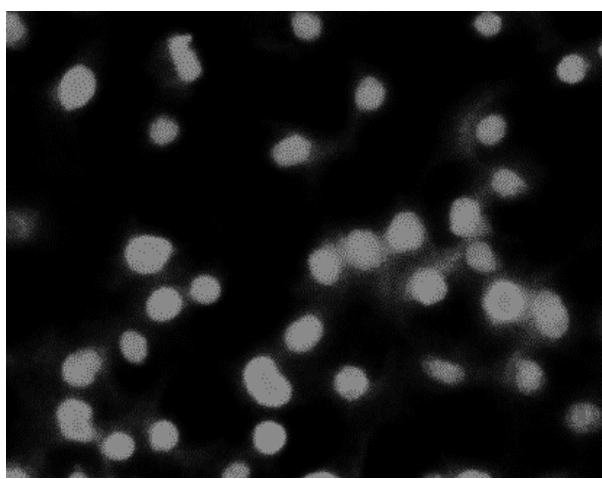
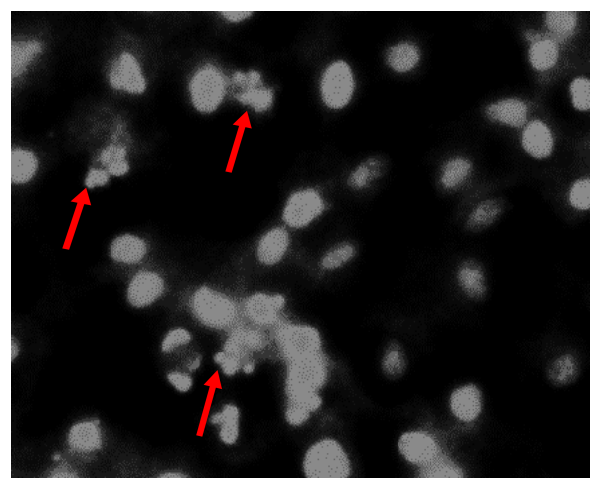


Fig. S19

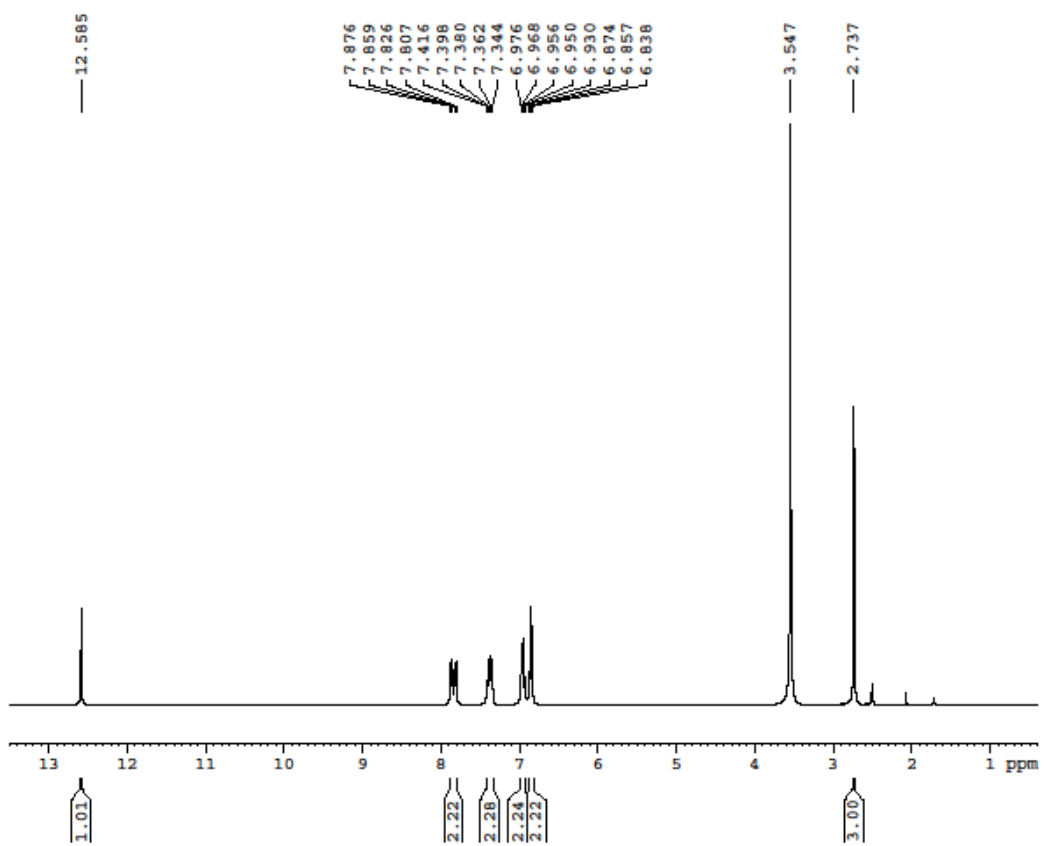


Control

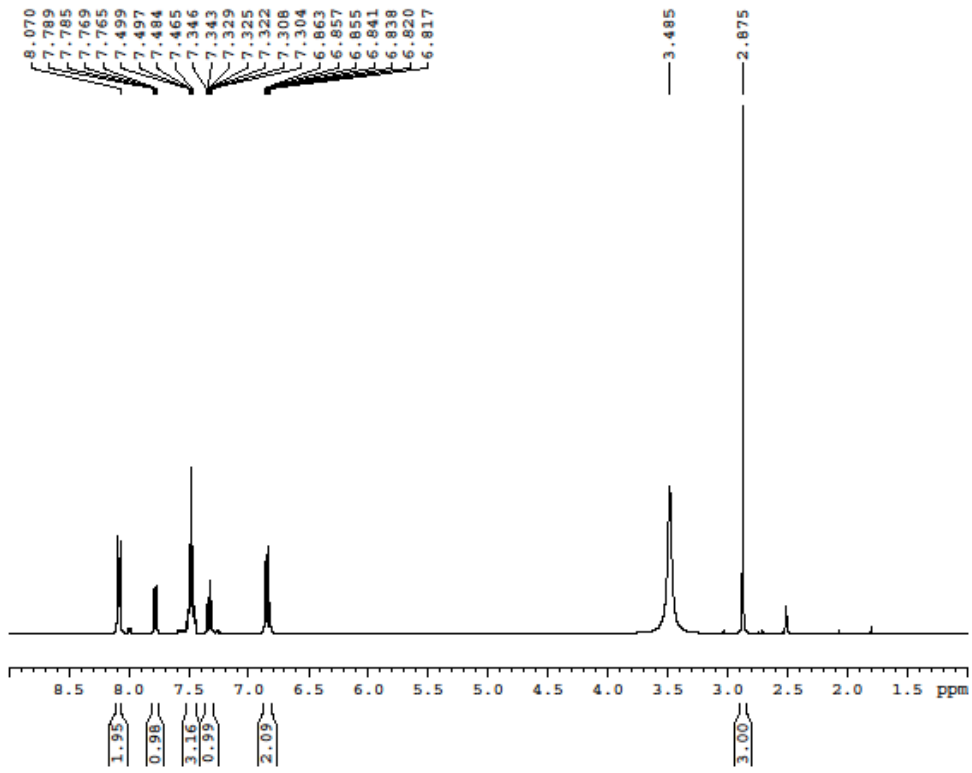


Ligand (H_2L^5) treated

Fig. S20



(a)



(b)

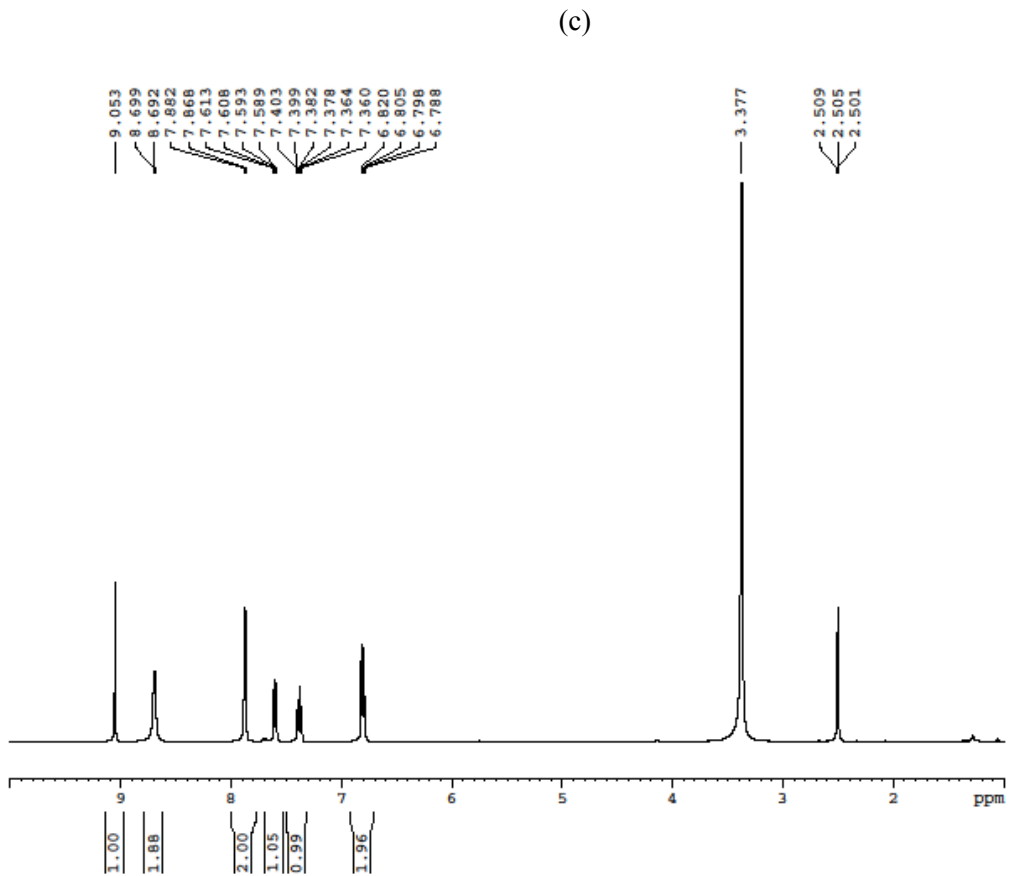
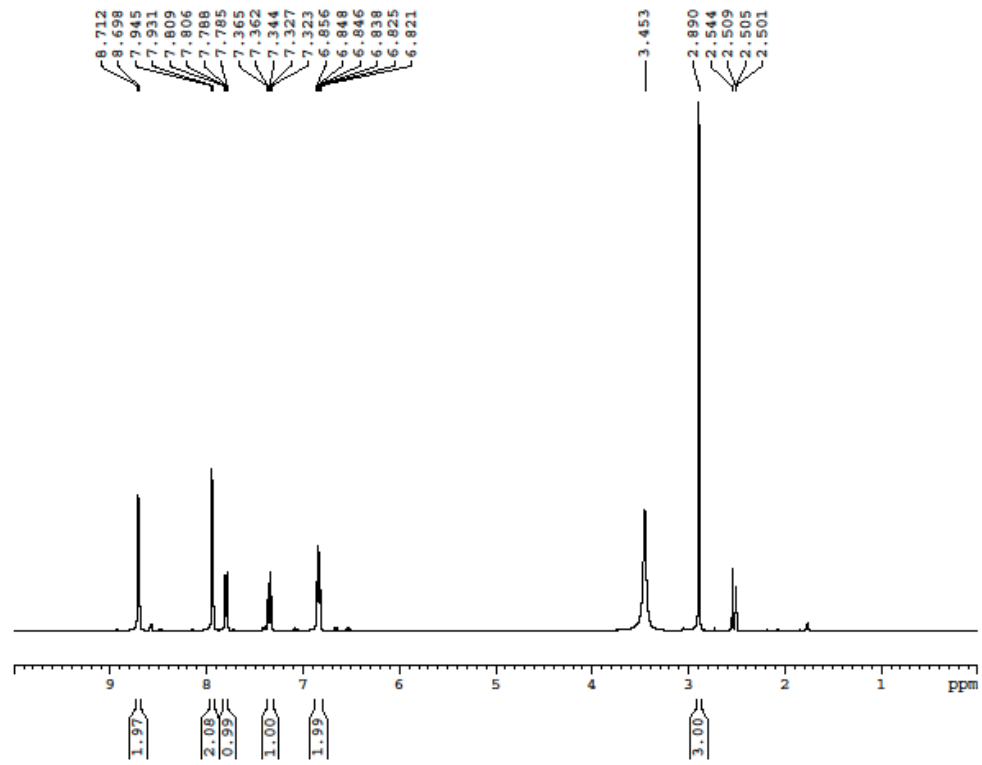


Fig. S21

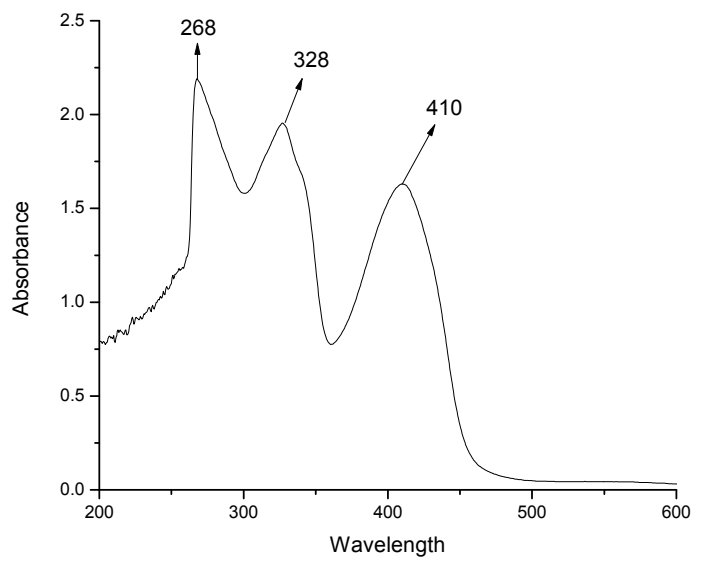


Fig. S22

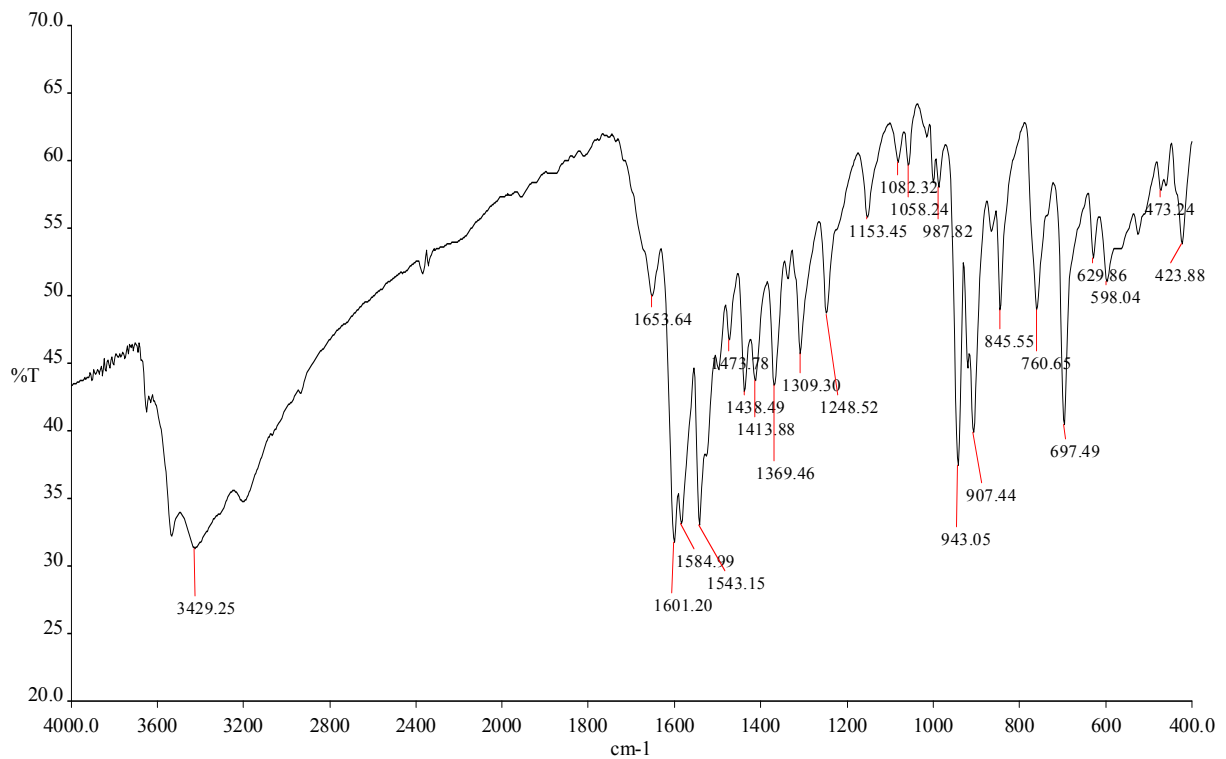


Fig. S23